Nano Materials Science 4 (2022) 44–51

Contents lists available at ScienceDirect

Nano Materials Science

journal homepage: www.keaipublishing.com/cn/journals/nano-materials-science/

Biaxial versus uniaxial strain tuning of single-layer MoS_2

Felix Carrascoso, Riccardo Frisenda **, Andres Castellanos-Gomez *

Materials Science Factory, Instituto de Ciencia de Materiales de Madrid (ICMM-CSIC), 28049, Madrid, Spain

ARTICLE INFO

Keywords:
2D materials
MoS2
Strain engineering
biaxial strain
uniaxial strain
reflectance spectra

ABSTRACT

Strain engineering has arisen as a powerful technique to tune the electronic and optical properties of two-dimensional semiconductors like molybdenum disulfide (MoS_2). Although several theoretical works predicted that biaxial strain would be more effective than uniaxial strain to tune the band structure of MoS_2, a direct experimental verification is still missing in the literature. Here we implemented a simple experimental setup that allows to apply biaxial strain through the bending of a cruciform polymer substrate. We used the setup to study the effect of biaxial strain on the differential reflectance spectra of 12 single-layer MoS_2 flakes finding a redshift of the excitonic features at a rate between −40 meV/% and −110 meV/% of biaxial tension. We also directly compare the effect of biaxial and uniaxial strain on the same single-layer MoS_2 finding that the biaxial strain gauge factor is 2.3 times larger than the uniaxial strain one.

1. Introduction

The outstanding combination of high resilience to mechanical deformations with rather strong strain-sensitive band structures makes two-dimensional (2D) semiconductors particularly suited for strain engineering [1–8]. These desirable properties have, indeed, triggered the interest of a great deal of the scientific community to research on the properties of 2D semiconductors under strain.

Molybdenum disulfide (MoS_2) is probably the most studied semiconductor to date [9–15] and several works focused on strain engineering [16–48]. Although many theoretical works predicted that biaxial strain can tune more effectively the band structure of MoS_2 [16–18,24,25,29,30,34,44], most of the experimental works only deal with the specific case of uniaxial strain [19,20,22,26–28,33,35,37–41,45–47,49,50]. To date, only a handful of experimental works explored the application of biaxial strain to atomically thin MoS_2 using piezoelectric substrates [21], thermal expansion mismatch [31,36,42,43,51], exploiting the presence of naturally occurring bubbles [48,52,53], the creation of artificial blisters [32,54,55] or bubbles [56–58], a thin film stressor method [59] or a capillary-pressure-induced nanoindentation method [60]. All these methods present some disadvantages (complexity, cross-talk, etc.) with respect to the beam-bending approach widespread to apply uniaxial strain, explaining the large number of works focused on uniaxial strain. Therefore, an experimental method that allows to control biaxial strain with a geometry similar to the beam bending method would be highly desirable. In 2015, Androulidakis et al. [61] adapted the macroscopic cruciform biaxial strain testing, used to probe the mechanical properties of standard materials, to apply biaxial strain to graphene. The method was based on the bending of a polymer substrate with cruciform shape through an indentation at its center. They applied this method to study the shift of Raman modes of graphene upon biaxial straining, but it has been overlooked by the community interested on strain engineering of 2D semiconductors (see the note after the conclusions).

Here we implement a simple experimental setup to apply biaxial strain to 2D materials, following the cruciform bending/indentation method, under the inspection of an optical microscope. We provide all the technical details to facilitate the replication of the setup by others, note that this relevant information was somewhat missing in Ref. [61] making it difficult adopting this technique by other experimental groups. We also modified a method recently developed to calibrate uniaxial straining setups [47] to calibrate the amount of biaxial strain achieved upon central indentation in the cruciform. We found that the calibration may strongly differ, depending on the specific dimensions of the cruciform, from the analytical formula used in Ref. [61] thus illustrating the relevance of performing an independent strain calibration. We then use the setup to strain 12 single-layer MoS_2 flakes finding that their reflectance spectra are red-shifted at a rate of −36 to −108 meV/% of biaxial tension. Interestingly, during the measurements we found that MoS_2 flakes are more prone to break during biaxial tensioning than during

* Corresponding author.
** Corresponding author.
E-mail addresses: Riccardo.frisenda@csic.es (R. Frisenda), Andres.castellanos@csic.es (A. Castellanos-Gomez).

https://doi.org/10.1016/j.nanoms.2021.03.001
Received 17 December 2020; Accepted 22 February 2021
Available online 16 March 2021

uniaxial tensioning (where the main failure mechanism is slippage). In many cases the breaking is followed by a sudden release of strain and further tensioning leads to a new red-shift of the reflectance spectra from the released position. We finally directly compare experimentally biaxial and uniaxial approaches by subjecting the same single-layer MoS_2 flake to successive biaxial and uniaxial tensioning cycles while monitoring the strain induced shift in the flake reflectance spectra. We experimentally verify that biaxial strain provides a more efficient way to tune the optical properties of MoS_2, as compared with uniaxial strain, in good agreement with theoretical predictions.

Fig. 1(a–d) show pictures of the experimental setup develop to controllably bend cruciform polymer substrates through a central indentation. The setup is based on a manual linear Z-stage positioner (MAZ-40-10, by Optics Focus) that allows accurate displacements in the vertical direction (the minimum division of the micrometer screw correspond to 10 μm displacement). Fig. 1(c and d) show an optical picture of a cruciform sample made of 100 μm thick Mylar placed onto the setup. Mylar is selected as substrate for the cruciform given its large Young's modulus (~4–5 GPa) as large strain transfer is obtained for substrates with a high Young's modulus [28,36] and it has been probed that a good strain transfer is already observed in substrates with a Young's modulus higher than 1 GPa [36,62]. Fig. 1(e–p) show the blueprints of the homebuilt parts employed to modify the linear manual stage. The blueprint of the bracket is shown in Fig. 1(e–h), it is the main part of the setup and the geometrical center of the flexible cruciform must be placed onto the center of its circular hole as illustrated in Fig. 1(c and d). Fig. 1(i–l) show the blueprint of the indenter, the hemisphere (Thorlabs PKFESP) placed on the top of this piece pushes the cruciform from the bottom and, therefore, it is symmetrically deformed in-plane [61]. The clamp, whose blueprint is shown in Fig. 1(m–p), is responsible for holding the arms of the cruciform and let them slide over it while the geometrical center of the cruciform is being pushed by the indenter.

In order to directly calibrate the amount of biaxial strain that can be applied, for a given central indentation of the cruciform, we adapted the calibration protocol developed to calibrate uniaxial straining setups [47]. Briefly, we pattern an array of pillars with photolithography on the

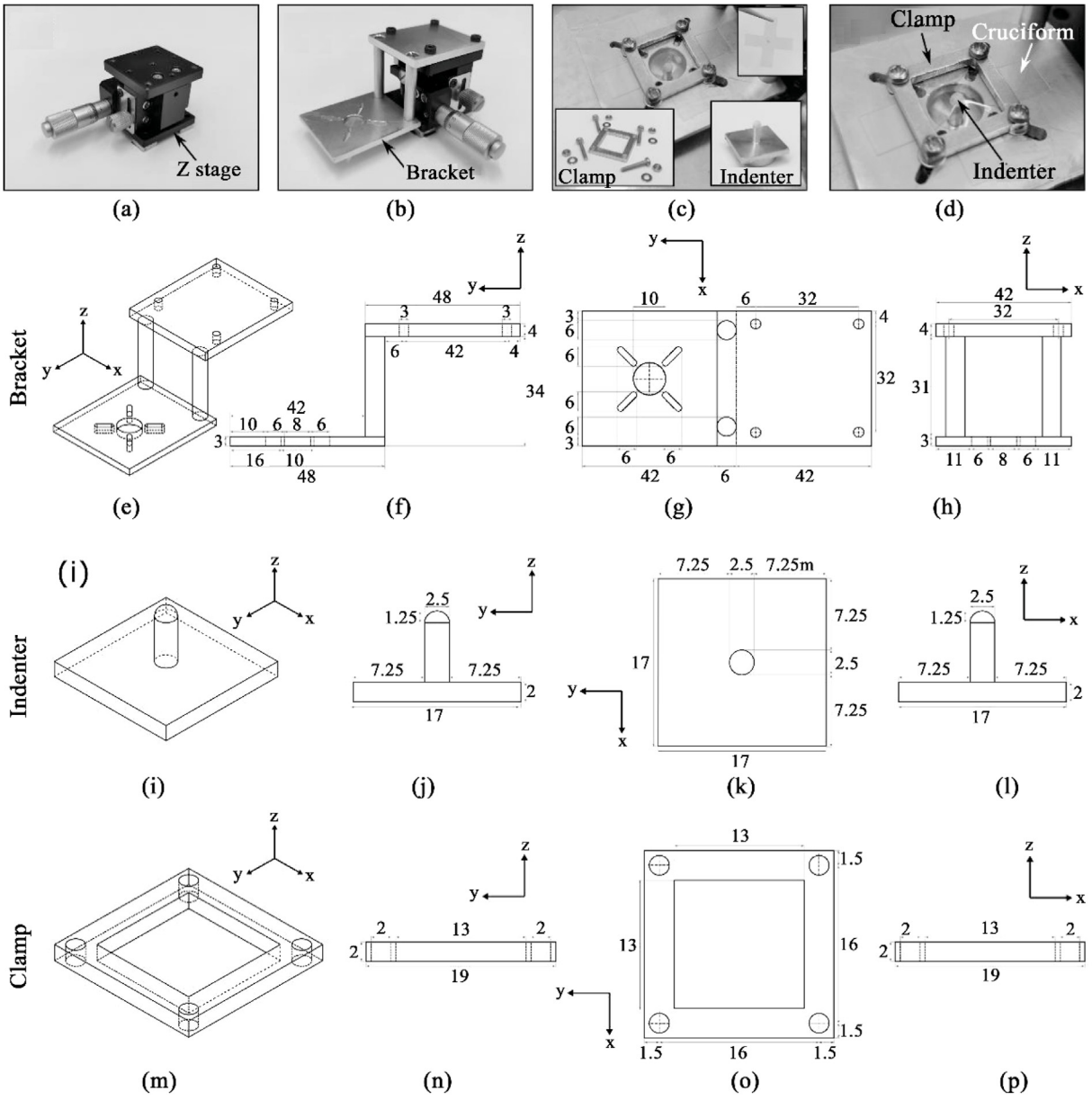

Fig. 1. Experimental setup for the bending/indentation of a cruciform polymer substrate for biaxial straining 2D materials. (a–d) Pictures of the experimental setup. (e–h) Blueprint of the bracket. (i–l) Blueprint of the indenter. (m–p) Blueprint of the clamp. (All dimensions in millimeters).

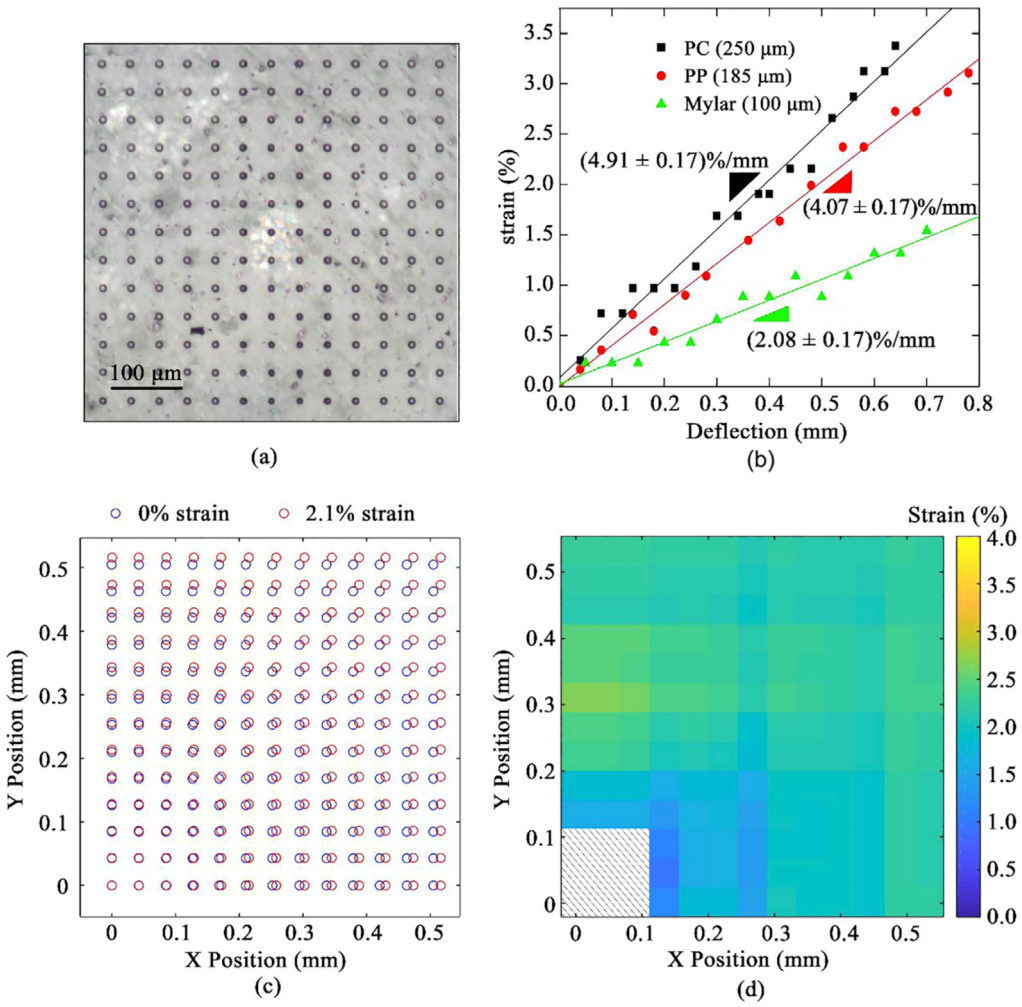

Fig. 2. Direct calibration of the applied biaxial strain. (a) Optical picture of the patterned pillars. (b) Biaxial strain calibration for different polymer substrates. (c) Extracted position of the pillars before and after applying strain. (d) Map of the spatial variation of the applied strain.

central part of the cruciform (Fig. 2a) and we acquire optical microscopy images of the pillar array at different displacements of the micrometer screw. The biaxial strain value for a given micrometer screw displacement can be determined by measuring the distance between the pillars from the optical images as the strain, it is defined as:

$$\varepsilon = \frac{L - L_0}{L_0}$$

where L_0 is the pillar distance at zero-strain and L at the given micrometer screw displacement.

Fig. 2b shows the resulting biaxial strain calibration traces measured for 3 different polymer substrates: polycarbonate (PC, 250 μm), polypropylene (PP, 185 μm) and Mylar (100 μm). Moreover, by extracting the position of each pillar in the images (Fig. 2c) one can even determine the spatial homogeneity of the applied biaxial strain and obtain a map of the spatial variation of the applied biaxial strain (Fig. 2d), within a 500 by 500 μm^2 area around the center of the cruciform, finding a small variability of (2.1 ± 0.2) % strain (histogram reported in the Supporting Information).

To fabricate the single-layer MoS_2 samples to be studied, a bulk MoS_2 crystal (Molly Hill mine, Quebec, Canada) is exfoliated with Nitto tape (SPV224) and the cleaved crystallites are then transferred onto a Gel-Film substrate (WF x 4 6.0 mil, by Gel-Pak®). Single-layer flakes are identified on the surface of the Gel-Film substrate by combination of quantitative analysis of transmission mode optical microscopy images [63,64] and micro-reflectance spectroscopy [65,66]. Once a suitable single-layer MoS_2 flake is identified, it is deterministically placed onto the geometrical center of a cruciform within ~10 μm accuracy through an all dry transfer method [67–69]. The inset in Fig. 3a shows a picture of a single-layer MoS_2 flake on a Mylar cruciform. We use differential micro-reflectance spectroscopy to probe the band structure changes induced by biaxial-strain on the single layer MoS_2 flake [66] (see Fig. 3a). The spectra have two prominent peak features arising from the resonances associated to the direct valence-to-conduction band transitions at the K point of the Brillouin zone that yields the generation of excitons (labelled A and B according to the most common nomenclature in the literature) [10,65,70–72]. Upon biaxial tension, both A and B peaks red shift. Fig. 3b shows the energy of the A and B peaks upon increasing biaxial strain. One can fit the excitons energy *vs.* strain dataset to a straight-line from whose slope the gauge factor, *i.e.* the excitons energy shift per % of biaxial tension, can be extracted. For the flake shown in Fig. 3a we find gauge factor values of −90.2 meV/% and −81.5 meV/% for the A and B excitons respectively. The insets in Fig. 3b show the statistical information obtained after measuring 12 different single-layer MoS_2 flakes. In these box-plots the dispersion of the obtained gauge factor can be observed. The box includes the data between the 25th and the 75th percentile, the middle line and small dot correspond to the median and the mean of the data, respectively, and the top and bottom lines correspond to the maximum and the minimum values, respectively. For A and B peaks, we found maximum gauge factor values of 108

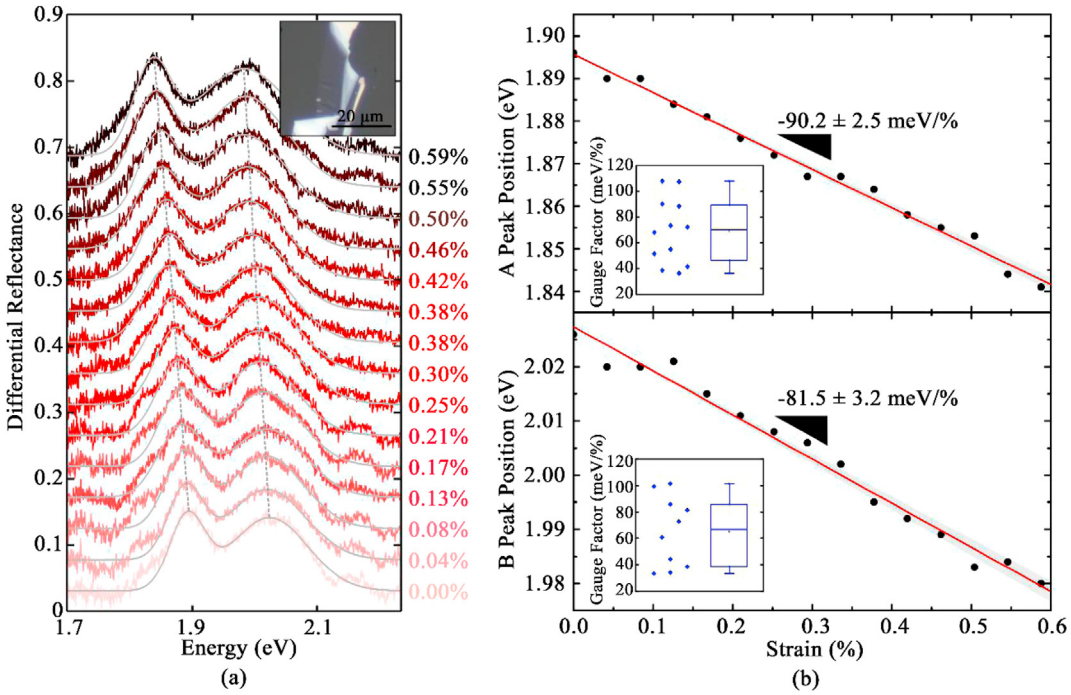

Fig. 3. Biaxial strain tuning the optical spectra of single-layer MoS_2. (a) Differential reflectance spectra at different biaxial strain values of a single layer MoS_2 flake. (Inset) Optical microscopy image of the single-layer MoS_2 flake subjected to biaxial straion. (b) A and B exciton energy positions as a function of biaxial strain. Insets show the statistical information of the gauge factors obtained for 12 different single-layer MoS_2 flakes.

Table 1
Summary of the experimental gauge factors obtained for biaxially strained MoS_2 in literature. * In the original work a gauge factor of 105 mev/% was estimated but it did not account for the intrinsic thermal contribution to the redshift. After discounting this intrinsic thermal contribution, the gauge factor is 4.2 meV/%.

Work	Strain Method	Measurement	Number of layers	Substrate	Maximum strain (%)	A exciton gauge factor (meV/%)
This work	Bending/indentation cruciform	Micro-reflectance	1L	Mylar	1.04	108
Hui et al. [21]	Piezoelectric substrates (compressive strain)	Photoluminescence and Raman	3L	PMN-PT (piezoelectric substrate)	0.2	300
Plechinger et al. [31]	Thermal expansion mismatch	Photoluminescence	1L	PDMS	0.2	4.2*
Frisenda et al. [36]	Thermal expansion mismatch	Micro-reflectance	1L	Polypropylene	1	51.1
Carrascoso et al. [43]	Thermal expansion mismatch	Micro-reflectance	2L	Polypropylene	0.87	41
Gant et al. [42]	Thermal expansion mismatch	Photocurrent spectroscopy	1L	Polycarbonate	−1.5 to 0.5	94
Kyoung Ryu et al.	Thermal expansion mismatch	Micro-reflectance	1L, 2L, 3L	Polypropylene	0.64	1L: 48 2L: 55 3L: 32
Guo et al. [48]	Naturally occurring bubbles	Photoluminescence and Raman	2L, 3L, 4L, 5L	SiO_2/Si	1 (in-plane strain)	2L, 3L, 5L: 107 4L: 114
Tyurnina et al. [52]	Naturally occurring bubbles	Photoluminescence	1L	MoS_2	2	55
Lloyd et al. [32]	Creation of artificial blisters	Photoluminescence	1L	SiO_2/Si	5.6	99
Blundo et al. [56]	Creation of artificial bubbles	Photoluminescence	1L	SiO_2/Si	2.1 (radial strain) 4.2 (in-plain strain)	37
Yang et al. [57]	Creation of artificial bubbles	Photoluminescence and Raman	1L, 2L, 3L	PDMS	9.4	1L: 41 2L: 27.3 3L: 30
Li et al. [60]	Capillary-pressure-induced nanoindentation	Photoluminescence and Raman	1L	SiO_2/Si	3	110
Michail et al. [73]	Bending/indentation cruciform	Photoluminescence and Raman	1L, 2L	PMMA	0.88	124 (1L exfoliated) 76 (1L CVD)

meV/% and 102 meV/%, respectively. Table 1 shows a summary of the reported experimental gauge factors for biaxially strained MoS_2 in the literature, as a comparison. One can see how the gauge factor obtained through this cruciform bending method is significantly larger to that obtained through exploiting the thermal expansion of polypropylene substrates, pointing out that the strain transfer on polypropylene could be lower than the calculated values (close to 100%) or might be temperature dependent.

It is worth mentioning that we found that single-layer MoS_2 flakes are prone to break upon biaxial strain tension, and that the breakdown comes

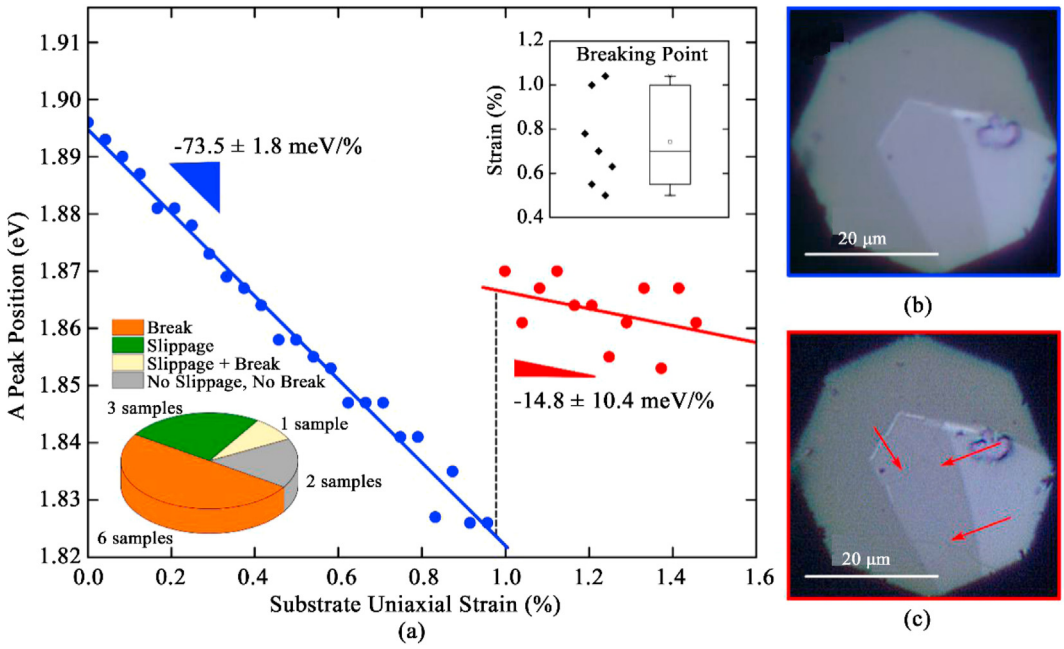

Fig. 4. Breakdown of single-layer MoS_2 flakes upon large biaxial strains. (a) A exciton energy values as a function of biaxial strain of a single-layer MoS_2 flake. At 1% one can observe strain releases. Inset shows the statistical information of the breaking/slipping point, extracted from the 12 single-layer MoS_2 measured flakes. (b) Optical microscopy image of the MoS_2 flake before cracking. (c) Optical image of the MoS_2 after cracking.

together with a sudden release of strain. Moreover, after cracking, one can typically keep strain-tuning the flake from the strain released energy position. This is in striking contrast to our previous observations in uniaxially strained TMDS flakes where the main source of failure during the straining tests was slippage that shows up as a drastic reduction of the strain gauge factor and hysteresis in the straining/releasing cycles. In Fig. 4, a single-layer MoS_2 flake is biaxially strained at high strain values. Fig. 4a shows the energy of the A peak while strain is increasing. At 1% strain, the flake cracks and the strain releases. After that, one can continue increasing the strain observing a new redshift of the excitons, with a different gauge factor, from the relaxed strain position. The bottom inset in Fig. 4a presents the statistical information about the number observed flakes that crack upon biaxial strain. Six flakes break at certain strain, while 3 slip without breaking and another one slip first and then

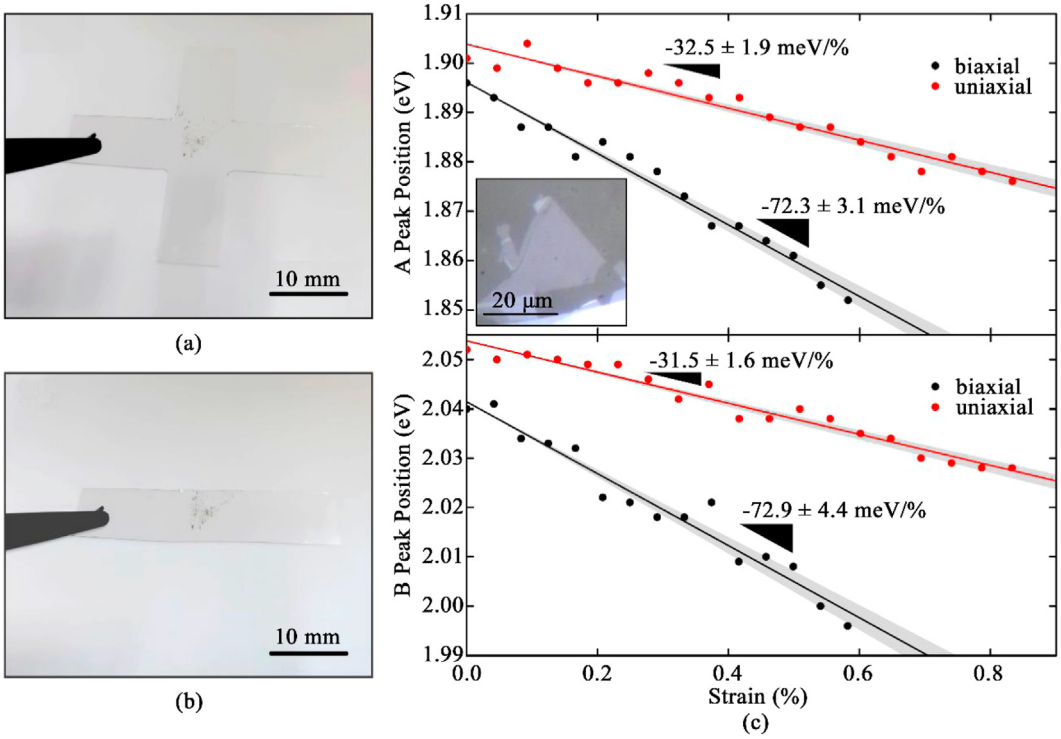

Fig. 5. Subjecting the same MoS_2 flake to biaxial and uniaxial strain. (a) Picture of a cruciform with transferred single-layer MoS_2 flake use to test a biaxial strain experiment. (b) Same sample after cutting two of its arms in order test uniaxial strain. (c) A and B exciton energy positions measured on the same single-layer MoS_2 flake at different biaxial and uniaxial strain values. (Inset) Optical microscopy image of the single-layer MoS_2 flake under study.

break. Two more flakes, subjected to a maximum strain of ~0.4% and 0.6% respectively, did not slip nor break. The top inset in Fig. 4a also shows the distribution of critical strain values for cracking observed in the 7 single-layer MoS_2 fakes that cracked upon straining where a mean strain value around 0.74% leads to the breakdown of the flakes. Fig. 4b and c shows the flake before and after cracking. The red arrows point to the cracks that appeared in the flake right after observing the strain release in Fig. 4a. Note that the biaxial strain induced shift of the excitons is reversible for strain loads below the slippage and failure strains. We address the reader to the Supp. Info. Fig. S2 for a dataset of a single-layer MoS_2 flake subjected to several strain loading/releasing cycles.

Finally, we have directly compared the effect of biaxial and uniaxial strain to tune the micro-reflectance spectra on the same single-layer MoS_2. We first measured a biaxial strain cycle on a single-layer MoS_2 flake transferred onto the center of a Mylar cruciform (Fig. 5a), similarly to Fig. 3. After the measurement, two of the cruciform arms are cut away, transforming the sample into a simple beam, as shown in Fig. 5b. We can then use a three-point bending test system [47] to subject the same single-layer MoS_2 to a uniaxial strain cycle. Fig. 5c shows the strain dependent energy of the A and B excitons measured on the same flake subjected to a biaxial tensioning (0.6%) and uniaxial tensioning cycle (0.8%). While the gauge factor for the biaxial straining measurements is ~70 meV/%, for the uniaxial strain case it only reaches ~30 meV/% (in good agreement with our recent statistical analysis based on 15 single-layer MoS_2 flakes subjected to uniaxial strain [47]). This improved strain tunability for biaxial strain is attributed to be due to the fact that biaxial tension increases the interatomic distance in all in-plane directions while uniaxial strain, due to the Poisson's effect, increases the interatomic distance in the loading direction while compressing the lattice in the in-plane orthogonal direction. This orthogonal compression upon uniaxial loading effectively reduces the gauge factor. This experiment is, to our knowledge, the first experimental validation of the stronger effect of biaxial strain, as compared to uniaxial strain, to tune the band structure of MoS_2, predicted by DFT calculations [16–18,24,25,29,30,34,44].

2. Conclusions

In summary, we present all the details to implement a simple experimental setup to subject 2D materials to biaxial strain and we describe a protocol to accurately calibrate the amount of applied biaxial strain. We have applied the setup to study the strain-induced changes in the differential reflectance spectra of 12 single-layer MoS_2 flakes, finding strain-induced spectral redshifts with gauge factors ranging from 35 meV/% to 110 meV/%. Interestingly, we found that large biaxial strain tends to break single-layer MoS_2 (while slippage is more common on uniaxial straining experiments), thus suddenly releasing the accumulated strain. We also directly compare the strain tuning effectivity of biaxial and uniaxial strain by subjecting the same single-layer MoS_2 flake to biaxial and uniaxial strain cycles. This measurement experimentally validates previous theoretical predictions as we find a biaxial strain gauge factor 2.3 times the uniaxial strain one. We believe that the results shown here can help the community working on strain engineering of 2D materials to employ more and more biaxial strain and thus to achieve higher strain-induced band structure tunability.

3. Note

During the elaboration of this manuscript we became aware of the work of Michail et al. [73] where they use the cruciform bending/indentation method developed by Androulidakis et al. [61], similar to this work, to study the effect of biaxial strain in the photoluminescence and Raman spectra of exfoliated and chemical vapour deposited single- and bi-layer MoS_2. In our work we provide complementary information, not present in Ref. [73]: 1) details about the experimental setup, 2) details about the calibration of the biaxial strain, 3) micro-reflectance measurements, 4) statistical analysis of the biaxial strain gauge-factor, 5) analysis of the strain-induced failure of the devices and 6) direct comparison between uniaxial and biaxial strain tuning.

Declaration of competing interest

The authors declare no competing financial interests.

Acknowledgements

This project has received funding from the European Research Council (ERC) under the European Union's Horizon 2020 research and innovation programme (grant agreement n° 755655, ERC-StG 2017 project 2D-TOPSENSE). R.F. acknowledges the support from the Spanish Ministry of Economy, Industry and Competitiveness through a Juan de la Cierva-formación fellowship 2017 FJCI2017-32919.

Appendix A. Supplementary data

Supplementary data to this article can be found online at https://doi.org/10.1016/j.nanoms.2021.03.001.

References

[1] R. Roldán, A. Castellanos-Gomez, E. Cappelluti, F. Guinea, Strain engineering in semiconducting two-dimensional crystals, J. Phys. Condens. Matter 27 (2015) 313201, https://doi.org/10.1088/0953-8984/27/31/313201.
[2] B. Amorim, A. Cortijo, F. de Juan, A.G. Grushin, F. Guinea, A. Gutiérrez-Rubio, H. Ochoa, V. Parente, R. Roldán, P. San-Jose, et al., Novel effects of strains in graphene and other two dimensional materials, Phys. Rep. 617 (2016) 1–54, https://doi.org/10.1016/j.physrep.2015.12.006.
[3] S. Deng, A.V. Sumant, V. Berry, Strain engineering in two-dimensional nanomaterials beyond graphene, Nano Today 22 (2018) 14–35, https://doi.org/10.1016/j.nantod.2018.07.001.
[4] Z. Dai, L. Liu, Z. Zhang, Strain engineering of 2D materials: issues and opportunities at the interface, Adv. Mater. 31 (2019) 1805417, https://doi.org/10.1002/adma.201805417.
[5] Y. Sun, K. Liu, Strain engineering in functional 2-dimensional materials, J. Appl. Phys. 125 (2019), https://doi.org/10.1063/1.5053795, 082402.
[6] T. Huang, W. Wei, X. Chen, N. Dai, Strained 2D layered materials and heterojunctions, Ann. Phys. 531 (2019) 1800465, https://doi.org/10.1002/andp.201800465.
[7] Z. Peng, X. Chen, Y. Fan, D.J. Srolovitz, D. Lei, Strain engineering of 2D semiconductors and graphene: from strain fields to band-structure tuning and photonic applications, Light Sci. Appl. 9 (2020) 190, https://doi.org/10.1038/s41377-020-00421-5.
[8] A. Chaves, J.G. Azadani, H. Alsalman, D.R. da Costa, R. Frisenda, A.J. Chaves, S.H. Song, Y.D. Kim, D. He, J. Zhou, et al., Bandgap engineering of two-dimensional semiconductor materials, npj 2D Mater. Appl. 4 (2020) 29, https://doi.org/10.1038/s41699-020-00162-4.
[9] K.F. Mak, C. Lee, J. Hone, J. Shan, T.F. Heinz, Atomically thin MoS2: a new direct-gap semiconductor, Phys. Rev. Lett. 105 (2010) 136805, https://doi.org/10.1103/PhysRevLett.105.136805.
[10] A. Splendiani, L. Sun, Y. Zhang, T. Li, J. Kim, C.-Y. Chim, G. Galli, F. Wang, Emerging photoluminescence in monolayer MoS $_2$, Nano Lett. 10 (2010) 1271–1275, https://doi.org/10.1021/nl903868w.
[11] A. Castellanos-Gomez, N. Agraït, G. Rubio-Bollinger, Optical identification of atomically thin dichalcogenide crystals, Appl. Phys. Lett. 96 (2010) 213116, https://doi.org/10.1063/1.3442495.
[12] Q.H. Wang, K. Kalantar-Zadeh, A. Kis, J.N. Coleman, M.S. Strano, Electronics and optoelectronics of two-dimensional transition metal dichalcogenides, Nat. Nanotechnol. 7 (2012) 699–712, https://doi.org/10.1038/nnano.2012.193.
[13] O.V. Yazyev, A. Kis, MoS 2 and semiconductors in the flatland, Mater. Today 18 (2015) 20–30, https://doi.org/10.1016/j.mattod.2014.07.005.
[14] A. Kuc, T. Heine, A. Kis, Electronic properties of transition-metal dichalcogenides, MRS Bull. 40 (2015) 577–584, https://doi.org/10.1557/mrs.2015.143.
[15] D. Lembke, S. Bertolazzi, A. Kis, Single-layer MoS 2 electronics, Acc. Chem. Res. 48 (2015) 100–110, https://doi.org/10.1021/ar500274q.
[16] E. Scalise, M. Houssa, G. Pourtois, V. Afanas'ev, A. Stesmans, Strain-induced semiconductor to metal transition in the two-dimensional honeycomb structure of MoS2, Nano Res 5 (2011) 43–48, https://doi.org/10.1007/s12274-011-0183-0.
[17] P. Johari, V.B. Shenoy, Tuning the electronic properties of semiconducting transition metal dichalcogenides by applying mechanical strains, ACS Nano 6 (2012) 5449–5456, https://doi.org/10.1021/nn301320r.
[18] H. Peelaers, C.G. Van De Walle, Effects of strain on band structure and effective masses in MoS2, Phys. Rev. B Condens. Matter 86 (2012) 241401, https://doi.org/10.1103/PhysRevB.86.241401.

[19] H.J. Conley, B. Wang, J.I. Ziegler, R.F. Haglund, S.T. Pantelides, K.I. Bolotin, Bandgap engineering of strained monolayer and bilayer MoS2, Nano Lett. 13 (2013) 3626–3630, https://doi.org/10.1021/nl4014748.

[20] K. He, C. Poole, K.F. Mak, J. Shan, Experimental demonstration of continuous electronic structure tuning via strain in atomically thin MoS2, Nano Lett. 13 (2013) 2931–2936, https://doi.org/10.1021/nl4013166.

[21] Y.Y. Hui, X. Liu, W. Jie, N.Y. Chan, J. Hao, Y.-T. Hsu, L.-J. Li, W. Guo, S.P. Lau, Exceptional tunability of band energy in a compressively strained trilayer MoS2 sheet, ACS Nano 7 (2013) 7126–7131, https://doi.org/10.1021/nn4024834.

[22] C.R. Zhu, G. Wang, B.L. Liu, X. Marie, X.F. Qiao, X. Zhang, X.X. Wu, H. Fan, P.H. Tan, T. Amand, et al., Strain tuning of optical emission energy and polarization in monolayer and bilayer MoS_{2}, Phys. Rev. B 88 (2013) 121301, https://doi.org/10.1103/PhysRevB.88.121301.

[23] V. Seshan, D. Ullien, A. Castellanos-Gomez, S. Sachdeva, D.H.K. Murthy, T.J. Savenije, H.A. Ahmad, T.S. Nunney, S.D. Janssens, K. Haenen, et al., Hydrogen termination of CVD diamond films by high-temperature annealing at atmospheric pressure, J. Chem. Phys. 138 (2013) 234707, https://doi.org/10.1063/1.4810866.

[24] H. Shi, H. Pan, Y.W. Zhang, B.I. Yakobson, Quasiparticle band structures and optical properties of strained monolayer MoS2 and WS2, Phys. Rev. B Condens. Matter 87 (2013) 155304, https://doi.org/10.1103/PhysRevB.87.155304.

[25] C.H. Chang, X. Fan, S.H. Lin, J.L. Kuo, Orbital analysis of electronic structure and phonon dispersion in MoS 2, MoSe2, WS2, and WSe2 monolayers under strain, Phys. Rev. B Condens. Matter 88 (2013) 195420, https://doi.org/10.1103/PhysRevB.88.195420.

[26] Y. Wang, C. Cong, C. Qiu, T. Yu, Raman spectroscopy study of lattice vibration and crystallographic orientation of monolayer mos2 under uniaxial strain, Small 9 (2013) 2857–2861, https://doi.org/10.1002/smll.201202876.

[27] C. Rice, R.J. Young, R. Zan, U. Bangert, D. Wolverson, T. Georgiou, R. Jalil, K.S. Novoselov, Raman-scattering measurements and first-principles calculations of strain-induced phonon shifts in monolayer MoS2, Phys. Rev. B Condens. Matter 87 (2013), https://doi.org/10.1103/PhysRevB.87.081307, 081307.

[28] Z. Liu, M. Amani, S. Najmaei, Q. Xu, X. Zou, W. Zhou, T. Yu, C. Qiu, A.G. Birdwell, F.J. Crowne, et al., Strain and structure heterogeneity in MoS2 atomic layers grown by chemical vapour deposition, Nat. Commun. 5 (2014) 5246, https://doi.org/10.1038/ncomms6246.

[29] D.M. Guzman, A. Strachan, Role of strain on electronic and mechanical response of semiconducting transition-metal dichalcogenide monolayers: an ab-initio study, J. Appl. Phys. 115 (2014) 243701, https://doi.org/10.1063/1.4883995.

[30] E. Scalise, M. Houssa, G. Pourtois, V.V. Afanasev, A. Stesmans, First-principles study of strained 2D MoS2, Phys. E Low-Dimensional Syst. Nanostructures 56 (2014) 416–421, https://doi.org/10.1016/j.physe.2012.07.029.

[31] G. Plechinger, A. Castellanos-Gomez, M. Buscema, H.S.J. van der Zant, G.A. Steele, A. Kuc, T. Heine, C. Schüller, T. Korn, Control of biaxial strain in single-layer molybdenite using local thermal expansion of the substrate, 2D Mater. 2 (2015), https://doi.org/10.1088/2053-1583/2/1/015006, 015006.

[32] D. Lloyd, X. Liu, J.W. Christopher, L. Cantley, A. Wadehra, B.L. Kim, B.B. Goldberg, A.K. Swan, J.S. Bunch, Band gap engineering with ultralarge biaxial strains in suspended monolayer MoS 2, Nano Lett. 16 (2016) 5836–5841, https://doi.org/10.1021/acs.nanolett.6b02615.

[33] X. He, H. Li, Z. Zhu, Z. Dai, Y. Yang, P. Yang, Q. Zhang, P. Li, U. Schwingenschlogl, X. Zhang, Strain engineering in monolayer WS2, MoS2, and the WS2/MoS2 heterostructure, Appl. Phys. Lett. 109 (2016) 173105.

[34] C.V. Nguyen, N.N. Hieu, Effect of biaxial strain and external electric field on electronic properties of MoS2 monolayer: a first-principle study, Chem. Phys. 468 (2016) 9–14, https://doi.org/10.1016/j.chemphys.2016.01.009.

[35] J.O. Island, A. Kuc, E.H. Diependaal, R. Bratschitsch, H.S.J. Van Der Zant, T. Heine, A. Castellanos-Gomez, Precise and reversible band gap tuning in single-layer $MoSe_2$ by uniaxial strain, Nanoscale 8 (2016), https://doi.org/10.1039/c5nr08219f.

[36] R. Frisenda, M. Drüppel, R. Schmidt, S. Michaelis de Vasconcellos, D. Perez de Lara, R. Bratschitsch, M. Rohlfing, A. Castellanos-Gomez, Biaxial strain tuning of the optical properties of single-layer transition metal dichalcogenides, npj 2D Mater. Appl. 1 (2017) 10, https://doi.org/10.1038/s41699-017-0013-7.

[37] I. Niehues, A. Blob, T. Stiehm, R. Schmidt, V. Jadriško, B. Radatović, D. Čapeta, M. Kralj, S.M. de Vasconcellos, R. Bratschitsch, Strain transfer across grain boundaries in MoS2 monolayers grown by chemical vapor deposition, 2D Mater. 5 (2018) 31003.

[38] I. Niehues, R. Schmidt, M. Drüppel, P. Marauhn, D. Christiansen, M. Selig, G. Berghäuser, D. Wigger, R. Schneider, L. Braasch, et al., Strain control of exciton-phonon coupling in atomically thin semiconductors, Nano Lett. 18 (2018), https://doi.org/10.1021/acs.nanolett.7b04868.

[39] I. Niehues, A. Blob, T. Stiehm, S.M. de Vasconcellos, Interlayer excitons in bilayer MoS2 under uniaxial tensile strain, Nanoscale 11 (27) (2019) 12788–12792.

[40] J.W. Christopher, M. Vutukuru, D. Lloyd, J.S. Bunch, B.B. Goldberg, D.J. Bishop, A.K. Swan, Monolayer MoS 2 strained to 1.3% with a microelectromechanical system, J. Microelectromechanical Syst. 28 (2019) 254–263.

[41] L. Mennel, M. Paur, T. Mueller, Second harmonic generation in strained transition metal dichalcogenide monolayers: MoS2, MoSe2, WS2, and WSe2, APL Photonics 4 (2019) 34404.

[42] P. Gant, P. Huang, D. Pérez de Lara, D. Guo, R. Frisenda, A. Castellanos-Gomez, A strain tunable single-layer MoS2 photodetector, Mater. Today 27 (2019) 8–13, https://doi.org/10.1016/j.mattod.2019.04.019.

[43] F. Carrascoso, D.-Y. Lin, R. Frisenda, A. Castellanos-Gomez, Biaxial strain tuning of interlayer excitons in bilayer MoS 2, J. Phys. Mater. 3 (2019), https://doi.org/10.1088/2515-7639/ab4432, 015003.

[44] K. Zollner, P.E.F. Junior, J. Fabian, Strain-tunable orbital, spin-orbit, and optical properties of monolayer transition-metal dichalcogenides, Phys. Rev. B 100 (2019) 195126, https://doi.org/10.1103/PhysRevB.100.195126.

[45] Z. Li, Y. Lv, L. Ren, J. Li, L. Kong, Y. Zeng, Q. Tao, R. Wu, H. Ma, B. Zhao, Efficient strain modulation of 2D materials via polymer encapsulation, Nat. Commun. 11 (2020) 1–8.

[46] A.P. John, A. Thenapparambil, M. Thalakulam, Strain-engineering the Schottky barrier and electrical transport on MoS 2, Nanotechnology 31 (2020) 275703.

[47] F. Carrascoso, H. Li, R. Frisenda, A. Castellanos-Gomez, Strain engineering in single-, bi- and tri-layer MoS2, MoSe2, WS2 and WSe2, Nano Res (2020), https://doi.org/10.1007/s12274-020-2918-2.

[48] Y. Guo, B. Li, Y. Huang, S. Du, C. Sun, H. Luo, B. Liu, X. Zhou, J. Yang, J. Li, et al., Direct bandgap engineering with local biaxial strain in few-layer MoS2 bubbles, Nano Res 13 (2020) 2072–2078, https://doi.org/10.1007/s12274-020-2809-6.

[49] R. Roldán, A. Castellanos-Gomez, E. Cappelluti, F. Guinea, Strain engineering in semiconducting two-dimensional crystals, J. Phys. Condens. Matter 27 (2015) 313201, https://doi.org/10.1088/0953-8984/27/31/313201.

[50] A. Castellanos-gomez, R. Rolda, E. Cappelluti, M. Buscema, F. Guinea, H.S. Zant, J. Van Der, G.A. Steele, Local strain engineering in atomically thin MoS_2, Nano Lett. 13 (2013) 5361–5366, https://doi.org/10.1021/nl402875m.

[51] Y.K. Ryu, F. Carrascoso, R. López-Nebreda, N. Agraït, R. Frisenda, A. Castellanos-Gomez, Microheater actuators as a versatile platform for strain engineering in 2D materials, Nano Lett. 20 (2020) 5339–5345, https://doi.org/10.1021/acs.nanolett.0c01706.

[52] A.V. Tyurnina, D.A. Bandurin, E. Khestanova, V.G. Kravets, M. Koperski, F. Guinea, A.N. Grigorenko, A.K. Geim, I.V. Grigorieva, Strained bubbles in van der Waals heterostructures as local emitters of photoluminescence with adjustable wavelength, ACS Photonics 6 (2019) 516–524, https://doi.org/10.1021/acsphotonics.8b01497.

[53] D. Tedeschi, E. Blundo, M. Felici, G. Pettinari, B. Liu, T. Yildrim, E. Petroni, C. Zhang, Y. Zhu, S. Sennato, et al., Controlled micro/nanodome formation in proton-irradiated bulk transition-metal dichalcogenides, Adv. Mater. 31 (2019) 1903795, https://doi.org/10.1002/adma.201903795.

[54] B. Liu, Q. Liao, X. Zhang, J. Du, Y. Ou, J. Xiao, Z. Kang, Z. Zhang, Y. Zhang, Strain-engineered van der Waals interfaces of mixed-dimensional heterostructure arrays, ACS Nano 13 (2019) 9057–9066, https://doi.org/10.1021/acsnano.9b03239.

[55] J. Chaste, A. Missaoui, S. Huang, H. Henck, Z. Ben Aziza, L. Ferlazzo, C. Naylor, A. Balan, A.T.C. Johnson, R. Braive, et al., Intrinsic properties of suspended MoS2 on SiO2/Si pillar arrays for nanomechanics and Optics, ACS Nano 12 (2018) 3235–3242, https://doi.org/10.1021/acsnano.7b07689.

[56] E. Blundo, M. Felici, T. Yildirim, G. Pettinari, D. Tedeschi, A. Miriametro, B. Liu, W. Ma, Y. Lu, A. Polimeni, Evidence of the direct-to-indirect band gap transition in strained two-dimensional WS 2 , MoS 2 , and WSe 2, Phys. Rev. Res. 2 (2020), https://doi.org/10.1103/physrevresearch.2.012024, 012024.

[57] R. Yang, J. Lee, S. Ghosh, H. Tang, R.M. Sankaran, C.A. Zorman, P.X.L. Feng, Tuning optical signatures of single- and few-layer MoS2 by blown-bubble bulge straining up to fracture, Nano Lett. 17 (2017) 4568–4575, https://doi.org/10.1021/acs.nanolett.7b00730.

[58] H. Luo, X. Li, Y. Zhao, R. Yang, Y. Hao, Y. Gao, N.N. Shi, Y. Guo, G. Liu, L. Zhao, et al., Simultaneous generation of direct- and indirect-gap photoluminescence in multilayer MoS2 bubbles, Phys. Rev. Mater. 4 (2020), https://doi.org/10.1103/PhysRevMaterials.4.074006.

[59] T. Peña, S.A. Chowdhury, A. Azizimanesh, A. Sewaket, H. Askari, S.M. Wu, Strain Engineering 2D MoS$_{2}$ with Thin Film Stress Capping Layers, 2020.

[60] H. Li, A.W. Contryman, X. Qian, S.M. Ardakani, Y. Gong, X. Wang, J.M. Weisse, C.H. Lee, J. Zhao, P.M. Ajayan, et al., Optoelectronic crystal of artificial atoms in strain-textured molybdenum disulphide, Nat. Commun. 6 (2015) 7381, https://doi.org/10.1038/ncomms8381.

[61] C. Androulidakis, E.N. Koukaras, J. Parthenios, G. Kalosakas, K. Papagelis, C. Galiotis, Graphene flakes under controlled biaxial deformation, Sci. Rep. 5 (2015) 1–11, https://doi.org/10.1038/srep18219.

[62] Q. Zhao, R. Frisenda, T. Wang, A. Castellanos-Gomez, InSe: a two-dimensional semiconductor with superior flexibility, Nanoscale 11 (2019) 9845–9850, https://doi.org/10.1039/C9NR02172H.

[63] N.S. Taghavi, P. Gant, P. Huang, I. Niehues, R. Schmidt, S. Michaelis de Vasconcellos, R. Bratschitsch, M. García-Hernández, R. Frisenda, A. Castellanos-Gomez, Thickness determination of MoS2, MoSe2, WS2 and WSe2 on transparent stamps used for deterministic transfer of 2D materials, Nano Res 12 (2019) 1691–1695, https://doi.org/10.1007/s12274-019-2424-6.

[64] C. Backes, A.M. Abdelkader, C. Alonso, A. Andrieux-Ledier, R. Arenal, J. Azpeitia, N. Balakrishnan, L. Banszerus, J. Barjon, R. Bartali, Production and processing of graphene and related materials, 2D Mater. 7 (2020) 22001.

[65] Y. Niu, S. Gonzalez-Abad, R. Frisenda, P. Marauhn, M. Drüppel, P. Gant, R. Schmidt, N. Taghavi, D. Barcons, A. Molina-Mendoza, et al., Thickness-dependent differential reflectance spectra of monolayer and few-layer MoS2, MoSe2, WS2 and WSe2, Nanomaterials 8 (2018) 725, https://doi.org/10.3390/nano8090725.

[66] R. Frisenda, Y. Niu, P. Gant, A.J. Molina-Mendoza, R. Schmidt, R. Bratschitsch, J. Liu, L. Fu, D. Dumcenco, A. Kis, et al., Micro-reflectance and transmittance spectroscopy: a versatile and powerful tool to characterize 2D materials, J. Phys. D Appl. Phys. 50 (2017), https://doi.org/10.1088/1361-6463/aa5256, 074002.

[67] A. Castellanos-Gomez, M. Buscema, R. Molenaar, V. Singh, L. Janssen, H.S.J. van der Zant, G.A. Steele, Deterministic transfer of two-dimensional materials by all-dry viscoelastic stamping, 2D Mater. 1 (2014), https://doi.org/10.1088/2053-1583/1/1/011002, 011002.

[68] R. Frisenda, E. Navarro-Moratalla, P. Gant, D. Pérez De Lara, P. Jarillo-Herrero, R.V. Gorbachev, A. Castellanos-Gomez, Recent progress in the assembly of nanodevices and van der Waals heterostructures by deterministic placement of 2D materials, Chem. Soc. Rev. 47 (2018) 53–68, https://doi.org/10.1039/C7CS00556C.

[69] Q. Zhao, T. Wang, Y.K.Y.K. Ryu, R. Frisenda, A. Castellanos-Gomez, An inexpensive system for the deterministic transfer of 2D materials, J. Phys. Mater. 3 (2020), https://doi.org/10.1088/2515-7639/ab6a72, 016001.

[70] K.F. Mak, C. Lee, J. Hone, J. Shan, T.F. Heinz, Atomically thin MoS_2: a new direct-gap semiconductor, Phys. Rev. Lett. 105 (2010) 136805, https://doi.org/10.1103/PhysRevLett.105.136805.

[71] A. Chernikov, T.C. Berkelbach, H.M. Hill, A. Rigosi, Y. Li, O.B. Aslan, D.R. Reichman, M.S. Hybertsen, T.F. Heinz, Exciton binding energy and nonhydrogenic rydberg series in monolayer WS 2, Phys. Rev. Lett. 113 (2014), https://doi.org/10.1103/PhysRevLett.113.076802, 076802.

[72] A. Castellanos-Gomez, J. Quereda, H.P. van der Meulen, N. Agraït, G. Rubio-Bollinger, Spatially resolved optical absorption spectroscopy of single- and few-layer MoS 2 by hyperspectral imaging, Nanotechnology 27 (2016) 115705, https://doi.org/10.1088/0957-4484/27/11/115705.

[73] A. Michail, D. Anestopoulos, N. Delikoukos, J.N. Parthenios, S. Grammatikopoulos, S. Tsirkas, N.N. Lathiotakis, O. Frank, K. Filintoglou, K. Papagelis, Biaxial strain engineering of CVD and exfoliated single- and bi-layer MoS 2 crystals, 2D Mater. (2020), https://doi.org/10.1088/2053-1583/abc2de.